Chapter 4

ABERRATIONS OF THE HUMAN EYE IN VISIBLE AND NEAR INFRARED ILLUMINATION.

This chapter is based on the article by Llorente, L. et al.,"Aberrations of the human eye in visible and near infrared illumination", Optometry and Vision Science 80, 26-35 (2003). The coauthors of the study are: Luis Díaz-Santana, David Lara Saucedo and Susana Marcos. The contribution of the author of this thesis to the study was the participation in the data collection and processing at Instituto de Óptica (LRT), as well as data and statistical analysis (HS and LRT).

4.1.- ABSTRACT

PURPOSE: To compare optical aberration measurements using IR (787 nm) and visible light (543 nm) in a heterogeneous group of subjects in order to assess whether aberrations are similar in both wavelengths and to estimate experimentally the ocular chromatic focus shift.

METHODS: Ocular aberrations were measured in near IR and visible light using LRT and HS wavefront sensor. Measurements were conducted on 36 eyes in total (25 and 11 eyes respectively), within a wide range of ages (20 to 71), refractive errors (-6.00 to +16.50 D) and optical quality

(RMS, excluding defocus, from 0.40 to 9.89 μm). The Zernike coefficients and the RMS corresponding to different terms between IR and green illumination were compared.

RESULTS: A Student t-test performed on the Zernike coefficients indicates that defocus was significantly different in all of the subjects but one. Average focus shift found between 787 nm and 543 nm was 0.72 D. A very small percentage of the remaining coefficients was found to be significantly different: 4.7% of the 825 coefficients (25 eyes × 33 terms) for LRT and 18.2% of the 275 coefficients (11 eyes × 25 terms) for HS. Astigmatism was statistically different in 8.3% of the eyes, RMS for 3rd order aberrations in 16.6%, and SA (Z_4^0) in 11.1%.

CONCLUSIONS: Aerial images captured using IR and green light showed noticeable differences. Apart from defocus, this did not affect centroid computations since, within the variability of the techniques, estimates of aberrations with IR were equivalent to those measured in green. In normal eyes, the LCA of the Indiana Chromatic Eye Model can predict the defocus term changes measured experimentally, although the intersubject variability could not be neglected. The largest deviations from the prediction were found on an aphakic eye and on the oldest subject.

4.2.- INTRODUCTION

Most of the currently available wavefront sensing techniques use IR illumination, due to the advantages that it presents over visible light (Chapter 1, section 1.2.5.2). However, for direct comparison between optical measurements (estimated from the wave aberration) and visual performance the equivalence between results obtained using IR and visible light has to be assured. Particularly, knowledge of the defocus shift between IR and visible wavelengths is essential if the results are to be used

to predict refraction. It is therefore essential to confirm that aberrations measured with IR and green light are equivalent, and to verify whether the focus difference between IR and green predictable by the LCA, and therefore reasonably predictable across subjects.

Previous measurements of aberrations at different visible wavelengths (450 through 650 nm) using a psychophysical technique (SRR) showed slight differences in some aberration terms as a function of wavelength (Marcos et al., 1999). The chromatic difference of focus they found agreed with previous psychophysical results from the literature. Previous studies (Lopez-Gil and Artal., 1997, Lopez-Gil and Howland, 1999) using reflectometric techniques to compare measured optical quality in visible (545 and 633 nm, respectively) and near IR (780 nm) did not find differences in HOA. Double-pass measurements (Santamaría et al., 1987) of MTFs in IR and green light appear to be similar, although subtraction of background halos (noticeably different between IR and green) was critical (Lopez-Gil and Artal., 1997). Another study using an objective crossed-cylinder aberroscope to measure aberrations reported that aberrations are virtually identical in near IR and green light (Lopez-Gil and Howland, 1999). However, the data analysis was mainly qualitative and limited to three eyes. Recent studies have expanded the wavelength range experimentally studied either towards the ultraviolet (Manzanera et al., 2008) or the IR boundaries (Fernandez and Artal, 2008, Fernandez et al., 2005). They confirm that monochromatic aberrations hardly change with wavelength, except for defocus, as found in the study reported in this chapter. They also studied how accurately their data fit the predictions of the LCA from theoretical equations, although only a few subjects were measured.

In this chapter ocular aberrations between near IR (786 nm for LRT and 788 nm for HS) and visible illumination (543 nm) are compared. Aberrations were measured with two objective experimental setups, LRT

and HS (see sections 2.2 in Chapter 2 and 3.3.2.1 in Chapter 3, respectively), although the conclusions drawn here can be extrapolated to unrelated commercially available instruments, based on similar principles. Measurements were performed on 36 subjects, with a wide range of ages, refractions, and ocular conditions (including old and surgical eyes), thus covering a wide range of aberrations, and potentially ocular and retinal structural differences. In addition, the intensity distribution of the aerial images obtained with both wavelengths were compared.

4.3.- METHODS

4.3.1.- LASER RAY TRACING

4.3.1.1.- Setup and procedures.

For this study, the device LRT1 (Moreno-Barriuso et al., 2001) (see Chapter 2, section 2.1) was used to measure ocular aberrations. Figure 4.1 shows the particular implementation for this study, which included a 543 nm He-Ne laser beam (Melles Griot, Alburquerque, USA; 5mW), and 785 nm diode IR laser beam co-aligned (Schäfter + Kirchhoff, Hamburg, Germany; 15mW).

4.3.1.2.- Setting and control experiment

Measurements were conducted following the protocol described in section 1.4, Chapter 1. Previous to the measurements, the system was calibrated to verify that it did not introduce chromatic aberration (see section 2.3.7 (b), Chapter 2).

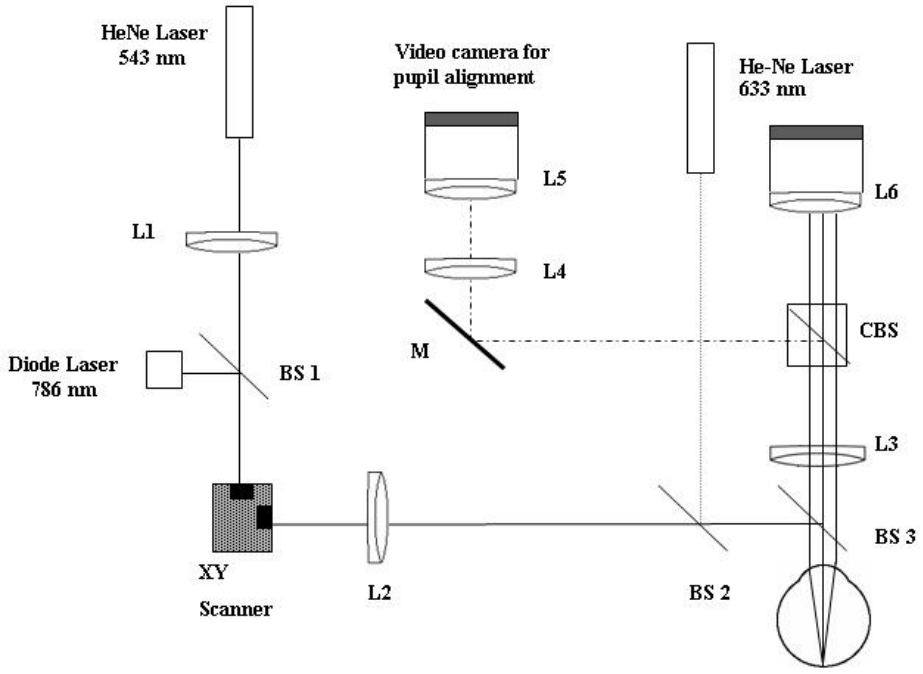

Figure 4.1. Schematic diagram of LRT1, used in this study .

A He-Ne (543 nm) laser or a diode laser (786 nm) samples the pupil plane and, simultaneously, light reflected off the retina is captured by a CCD camera. A red He-Ne laser (633 nm) acts as a fixation point. A video camera monitors pupil centration. BS1 and BS2 are pellicle beam splitters, BS3 is a glass beam splitter, CBS is a cube beam splitter, M is a mirror and L indicates lens.

4.3.1.3.- Subjects.

Twenty-five eyes (#1-#25) from 16 subjects were measured. Nineteen eyes were normal, one eye was aphakic (#8), and 5 eyes had undergone LASIK refractive surgery (#5, #6, #10, #12, #13). Ages ranged from 20 to 71 years (mean±std, 33±11 years), spherical error ranged from -6.00 to +16.50 D (-1.62±4.42 D), and astigmatism ranged from 3.78 to 0.07 D (1.07±0.98D).

4.3.1.4.- Measurements

Measurements were performed under the same protocol specified in Chapter 2, section 2.4 for the two different conditions tested: green (543 nm) and near IR illumination (786 nm).

4.3.2.- HARTMANN-SHACK

4.3.2.1.- Setup and procedures.

A detailed description of a similar system can be found in Chapter 3 without the minor modifications introduced for this study. Figure 4.2 shows a schematic diagram of the HS wavefront sensor used in this study, including this modifications. For this study, light from an IR (788 nm) super-luminiscent diode (Anritsu, 10 μw) was introduced by means of a pellicle beam splitter and co-aligned to the green (543 nm) He Ne laser beam (Melles Griot, 1 mw) used in previous measurements. The He-Ne laser was spatially filtered and expanded prior to collimation, bringing the maximum power reaching the eye to less than 5 μw over an 8 mm diameter pupil. Further power reduction was achieved by reducing the beam diameter to 1.5 to 2 mm and by the use of neutral density filters before spatial filtering. The SLD power was largely reduced after fibre coupling (to about 10% of its maximum nominal power), further power reduction was electronically controlled with its driver. In all cases the maximum power reaching the eye was at least one order of magnitude below the safety limits (ANSI, 2000). The principle of the HS system as well as the particular characteristics of the HS sensor have been described in Chapter 1, Section 1.2.3 and Chapter 3, section 3.3.2.1, respectively, of this thesis. The pupil size was 6 mm.

4.3.2.2.- Setting and control experiment

Measurements were conducted at Imperial College of Science Technology and Medicine, London, United Kingdom. The system was calibrated to ensure that it did not introduce chromatic aberration. Two reference HS images using green and IR light were compared. The green reference was used to calculate the aberrations of the IR reference. The order of magnitude of every Zernike coefficient was always smaller than or equal to the stds of any series of ten measurements of ocular aberrations using only one wavelength. This procedure proves that no significant amount of chromatic aberration was introduced by the optics of the system.

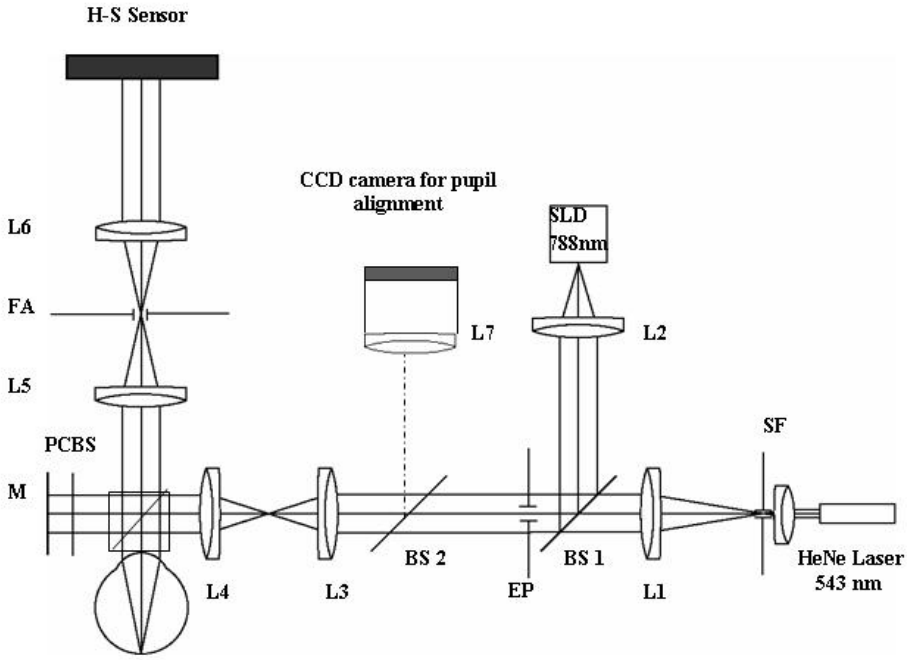

Figure 4.2. Schematic diagram of the HS wavefront sensor. Light coming from an expanded He-Ne (543 nm) laser or from a super luminescent diode (SLD) forms a point on the retina. SF is a spatial filter, and L1 and L2 are collimating lenses. L3, L4 and L5, L6 are relay systems in the illumination and imaging channels, respectively. EP is an entry pupil aperture (pupil diameter = 1.5 mm), and FA is a field aperture. Light reflected off the retina is imaged by a HS sensor (HS Sensor) on a cooled CCD camera. Images of the pupil are projected onto a CCD camera by objective lens L7 and monitors pupil centration. BS1 and BS2 are pellicle beam splitters, and PCBS is a polarizing cube beam splitter. M is a mirror that serves in reference image capture.

4.3.2.3.- Subjects.

Eleven 11 normal eyes (#26-#36) from 6 subjects were measured. Ages ranged from 22 to 26 years (23±1.47 years), spherical error ranged from –6.00 to +0.75 D (2.51±3.24 D) and astigmatism ranged from 0.07 to

4.00 D (1.30±1.57 D). The institutional research and ethical committee approved the use of the wavefront sensor and the experimental design. Written consent was obtained from all subjects participating in the study, according to the tenets of the Declaration of Helsinki. Pupils were dilated using Tropicamide 1% and Phenylephrine 2.5% 30 minutes prior to the beginning of the measurements.

4.3.2.4.- Measurements

Subjects were stabilized with the help of a dental impression and the pupil of the eye was aligned to the optical axis of the instrument, while it was continuously monitored with a CCD camera. The illumination source was used as the fixation point. Sphero-cylindrical refractive errors were compensated when necessary. At least six series of 10 HS images were collected, three using green illumination (543 nm) and the rest using IR illumination (788 nm). Images with the same wavelength were collected consecutively.

4.4.- RESULTS

4.4.1.- RAW DATA

Figure 4.3 A and Figure 4.3 B show a set of aerial images obtained with LRT for eye #5, for green and IR light respectively. Each image has been placed at the corresponding entry pupil position. The intensity patterns differ significantly across wavelengths. Figure 4.3 C shows the spot diagram corresponding to the average data of 3 consecutive runs with green light (crosses) and 4 consecutive runs with IR light (circles) for eye #5. The error bars indicate the std of the positions of the centroid between runs. Chromatic defocus was responsible for the consistent shift in the centroid locations between wavelengths, which increases with entry pupil eccentricity. Figure 4.3 D and Figure 4.3 E show HS images for green and IR light respectively, for eye #29. The presence of a halo surrounding

the centroid was more evident for the image with IR illumination than for that with green illumination. The spots at the upper right and the lower left corners of the image appear dimmer (particularly for green illumination) due to the use of crossed polarisation between illumination and recording (See Chapter 3, Section 3.4.2). Figure 4.3 F shows the HS centroids corresponding to D (crosses) and E (circles). As in LRT, the shift between the green and IR spots increases towards the periphery of the image.

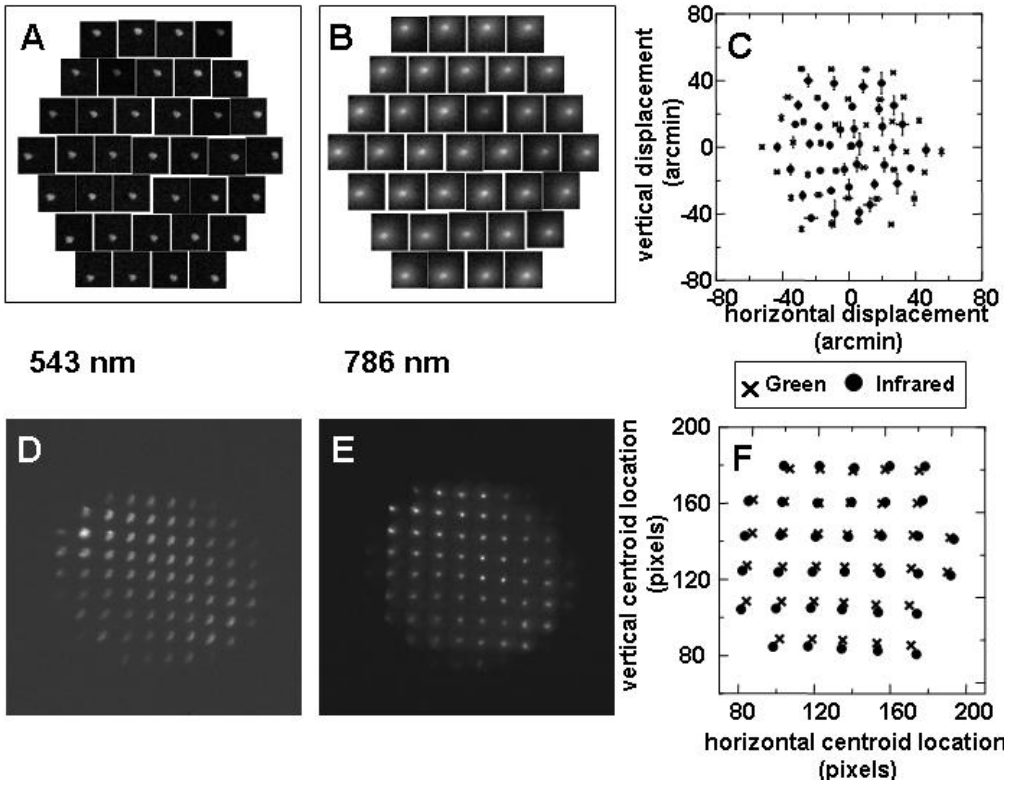

Figure 4.3. Raw data as obtained from LRT (panels A, B, and C) and HS wavefront sensor (panels D, E, and F).

In LRT, a series of retinal images is captured sequentially as a function of the entry pupil position. Aerial images obtained for eye #5 using green and IR light are shown in panels A and B, respectively. Panel C shows the corresponding spot diagram. Crosses represent green illumination, and circles represent IR illumination. Panels D and E show HS images for eye #29 for green and IR light, respectively. Panel F plots the corresponding centroids of the HS images. Symbol notation is the same as for panel C.

4.4.2.- *WAVE ABERRATION MAPS*

Figure 4.4 A shows wave aberration maps from LRT measurements for both wavelengths, for HOA. Eyes #9 and #22 were normal eyes, while #13 had undergone LASIK surgery. Each map is the average of at least three experimental runs. Contour lines are plotted every 0.2 μm. Figure 4.4 B shows wave aberration maps for three normal eyes (#29, #30 and #31) measured with HS for both wavelengths, excluding tilt and defocus. Contour lines are plotted every 0.5 μm. For both systems, the wave aberration patterns corresponding to green and IR wavelengths for the same subject are very similar.

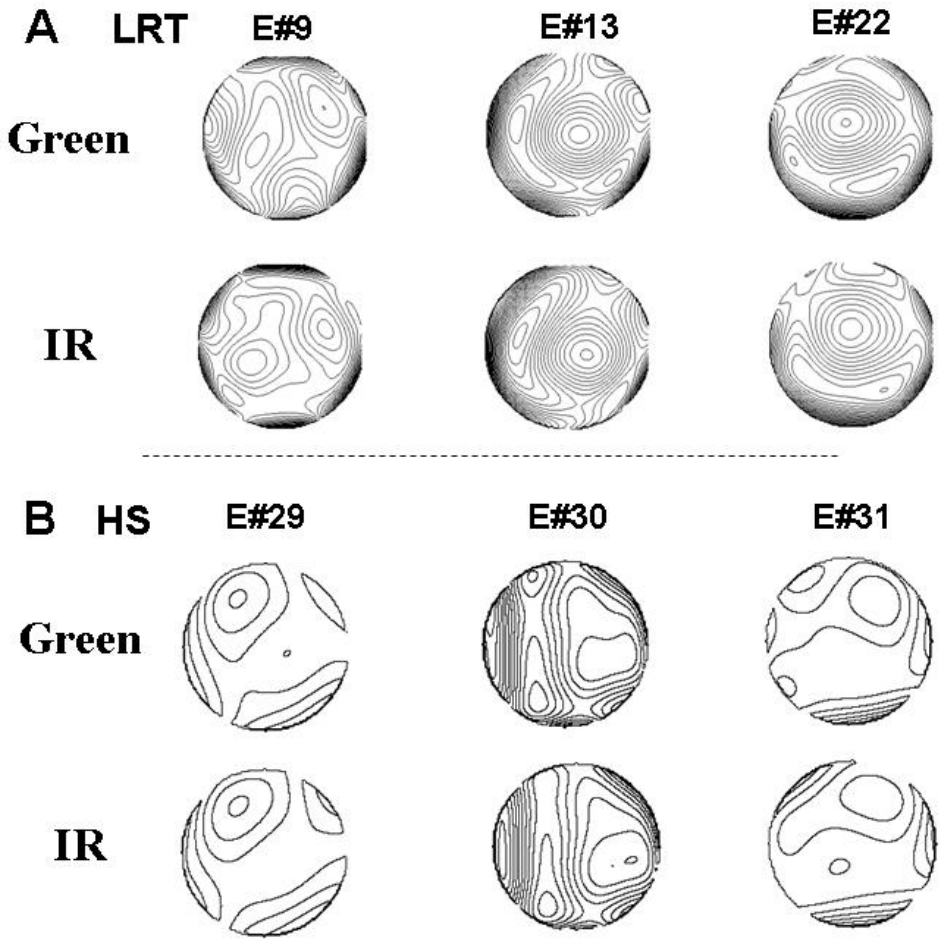

Figure 4.4. Wave aberration maps from LRT (A) and HS (B) for green and IR light.

A First- and second-order terms have been excluded. Eyes #9 and #22 were normal eyes, and #13 had undergone LASIK. Contour lines are plotted every 0.2 μm, and pupil size was 6.5 mm. B Tilts and defocus have been excluded. All three eyes were normal. Contour lines are plotted every 0.5 μm, and pupil size was 6 mm.

4.4.3.- ZERNIKE COEFFICIENTS AND RMS

Figure 4.5 shows plots of sets of Zernike coefficients for green (crosses) and IR (circles) light for the same eyes as in Figure 4.4. First and second order terms have been excluded to allow a higher resolution view of higher order terms. Error bars represent the std of the measurement. Mean variability (std), averaged across Zernike coefficients and subjects, was 0.10±0.06 (mean±std) for green light and 0.07±0.04 for IR light, for the measurements performed with LRT, and 0.019±0.009 (mean±std) for green light and 0.015±0.009 for IR light, for the measurements performed with HS. The differences between the Zernike coefficients measured with green and IR light, shown in Figure 4.5, are within the inherent variability of the techniques.

A univariate statistical analysis (Student t-test) on each Zernike coefficient for each eye was performed to detect which subjects and particular terms showed significant differences ($p<0.01$) when measured in green and IR light. For the 25 eyes measured with LRT 39 terms (excluding defocus) out of 825 (25 eyes x 33 terms), i.e. 4.7 %, were statistically different. The defocus term (Z_2^0) was statistically different in 24 of the 25 eyes (96% of the subjects). All the other statistically different terms were randomly distributed. For the 11 eyes measured with HS 61 terms out of 275 (11 eyes x 25 terms), i.e., 22% of the coefficients were statistically different. The defocus term was statistically different in all of the eyes. Among terms other than defocus, 50 out of 275 (18%) were found to be significantly different.

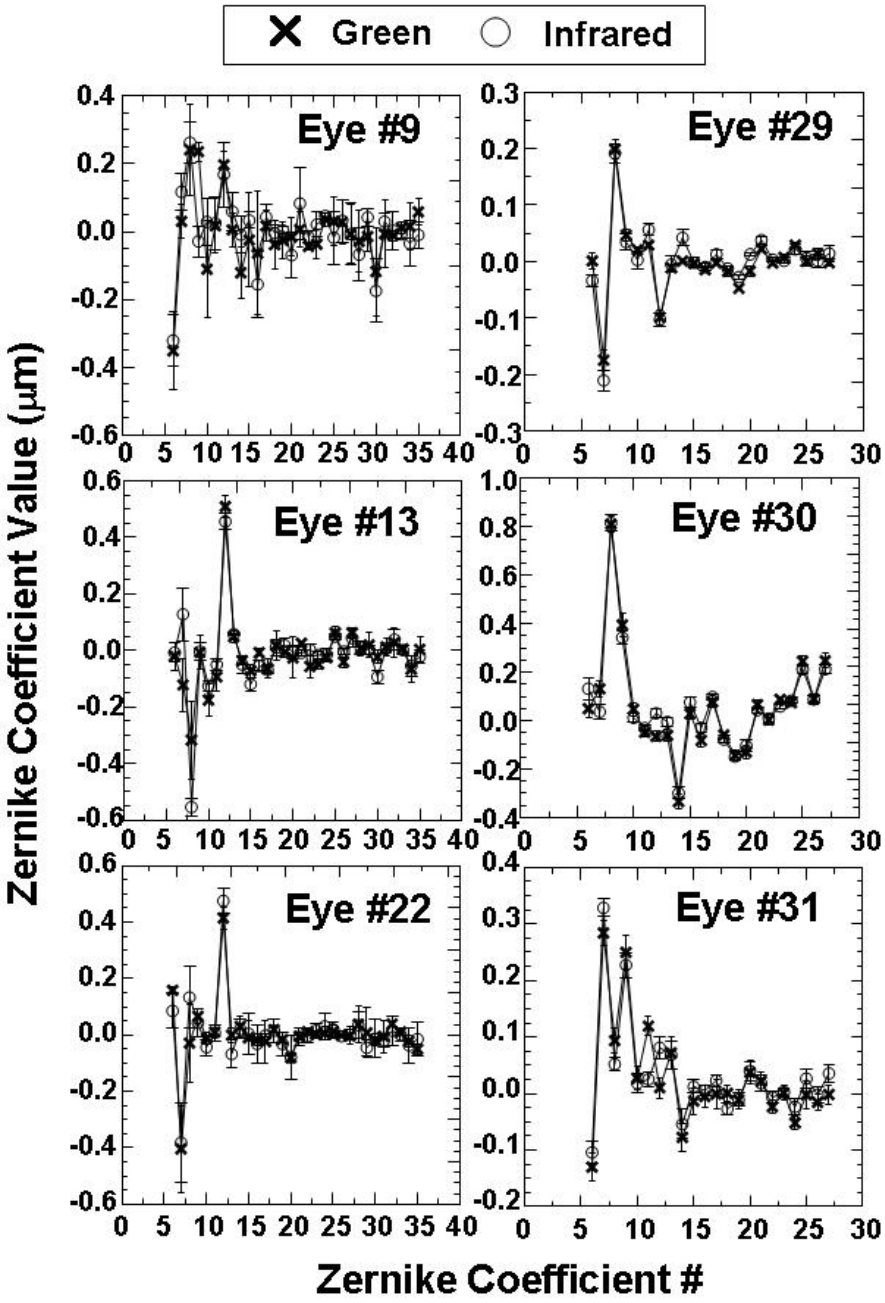

Figure 4.5. Plots of sets of the Zernike coefficients for green (crosses) and IR (circles) light for the same eyes as in Figure 4.4. First- and second-order terms have been cancelled. Error bars represent the std of the measurement.

Defocus for IR wavelength versus defocus for green wavelength in dioptres for all subjects is shown in Figure 4.6. There is a good linear correlation (R^2=0.98), and the slope of the linear fit is close to one (0.96). The focus shift between IR and green, given by the fitting equation is 0.72 D. The experimental focus shift was 0.78±0.29 D.

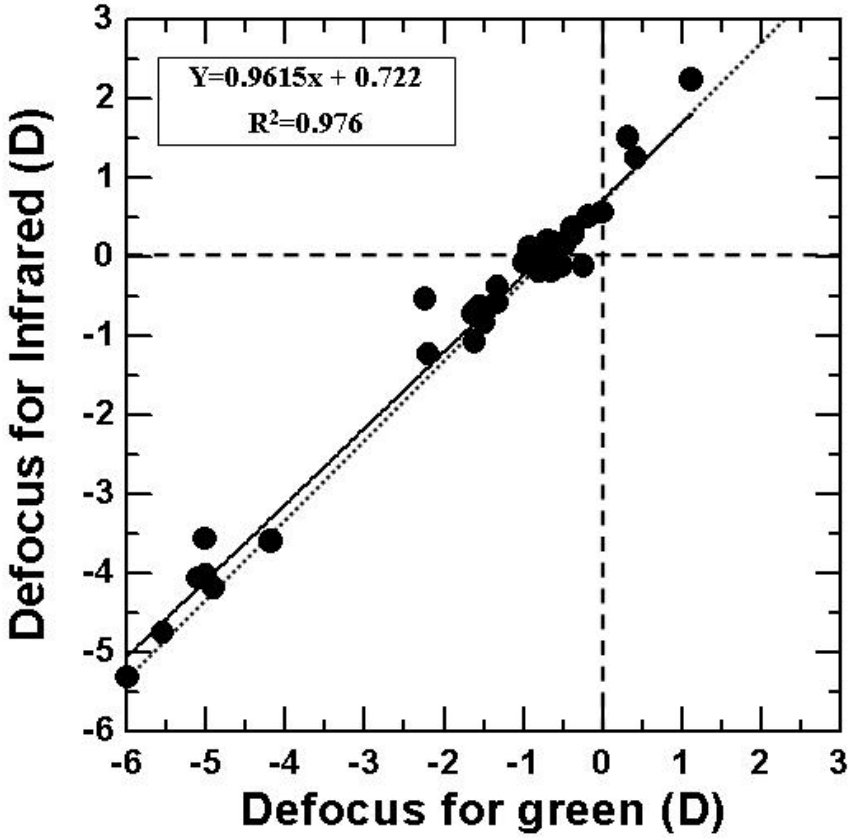

Figure 4.6. Defocus for IR vs. green wavelength in dioptres for all subjects.

The solid line represents the best linear fit to the data (R^2 = 0.976). The focus shift between infrared and green given by the fitting equation is 0.72 D. The slope of the linear fit is close to one (0.9615). The dashed line corresponds to a fitting line with slope equal to one and falls within the data variability

Bar diagrams in Figure 4.7 compare individual terms (astigmatism and SA) and the RMS including different terms, obtained with green (black bars) and IR (grey bars) for all subjects. Eyes #1 to #25 were measured with LRT, and #26 to #36 with HS. Asterisks indicate those eyes showing statistically significant differences ($p<0.01$). Astigmatism (Figure 4.7A) was statistically different in 3 of the 36 subjects (8.3 %). RMS for 3rd order aberrations (Figure 4.7 B) was statistically different in 6 of the 36 subjects (16.6 %). RMS for HOA (Figure 4.7 C) was statistically different in 5 of the 36 subjects (13.5 %). Spherical aberration (Z_4^0) (Figure 4.7 D) was statistically different in 4 of the 36 subjects (11.1%). Only one normal eye (#35) came out significantly different for all the terms or orders reported above (RMS for HOA, 3rd order aberrations, SA and astigmatism).

4.5.- DISCUSSION

This study shows that while the intensity distribution of LRT aerial images or HS images is notably different between green and IR illumination, both wavelengths provide aberration estimates within the experimental error (except for defocus). Our sample includes eyes with large differences in optical quality (from normal eyes to surgical eyes) and ages (20 through 71), suggesting that this conclusion holds for most of the population.

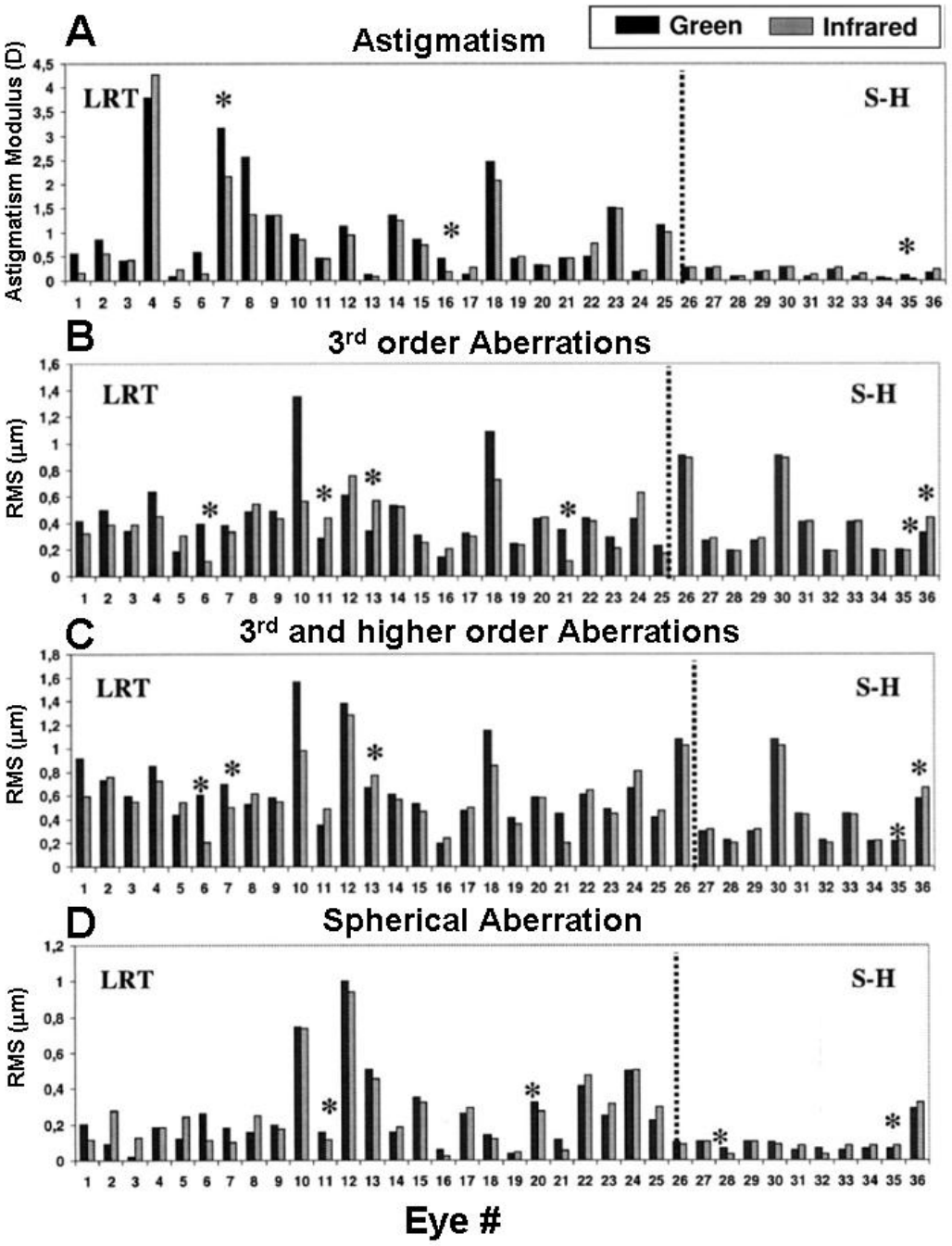

Figure 4.7. Bar diagrams comparing individual terms (astigmatism, A, and SA, D) and the root mean square wavefront error (RMS) for different orders (third order aberrations, B, and HOA, D), obtained with green (black bars) and IR (grey bars) for all subjects. Asterisks indicate the statistically different coefficients. Astigmatism was compensated during the measurement only for those eyes measured with HS.

4.5.1.- DIFFERENCES IN IMAGE INTENSITY PROFILES

Figure 4.3 shows relevant intensity differences between the aerial images obtained with IR and those obtained with green illumination. IR images are typically more spread and are surrounded by a broad halo. It has been suggested that most of the light contributing to the core of double-pass aerial images is probably due to the light captured and guided back from the photoreceptors (Lopez-Gil and Artal., 1997, Williams et al., 1994). The halo is probably produced by effects other than aberrations, such as retinal stray light scattered at the choroid (Westheimer and Campbell, 1962, Westheimer and Liang, 1995). Retinal scattering increases for longer wavelengths due to their deeper penetration within the retina and the choroid (Elsner et al., 1992, Gorrand et al., 1984).

Some previous comparisons of optical quality in IR and green light were based on estimates from double-pass aerial images. A computer simulation was performed to evaluate the contribution to the aerial image spread caused by degradation other than the ocular aberrations, and the influence of wavelength on this additional contribution. LRT double-pass aerial images were simulated from the estimated wave aberration function. LRT aerial images are the cross-correlation of the entry (1st pass) and exit (2nd pass) PSF. The entry pupil is a narrow incoming Gaussian beam (variance=0.10 mm and = 0.13 mm respectively, for green and IR illumination) and the exit pupil is a 3-mm circular pupil. The entry and exit pupil sizes correspond to the experimental values in the LRT setup. Insets in Figure 4.8 show real images and simulated images, corresponding to an entry pupil centered at coordinates (+1.5, -2.6 mm). Figure 4.8 A and Figure 4.8 B show experimental and simulated results for green and IR light respectively, for eye #22. The plots represent the normalized radial intensity profile of the corresponding real (solid) and simulated (dashed) aerial images. The distance from the peak position to

the zero position represents the centroid deviation from the chief ray (which is practically the same for the simulated and real images). The width of the simulated images accounts for the spread caused exclusively by the measured aberrations, while the real images are further enlarged by scattering and non-measured higher-order aberrations.

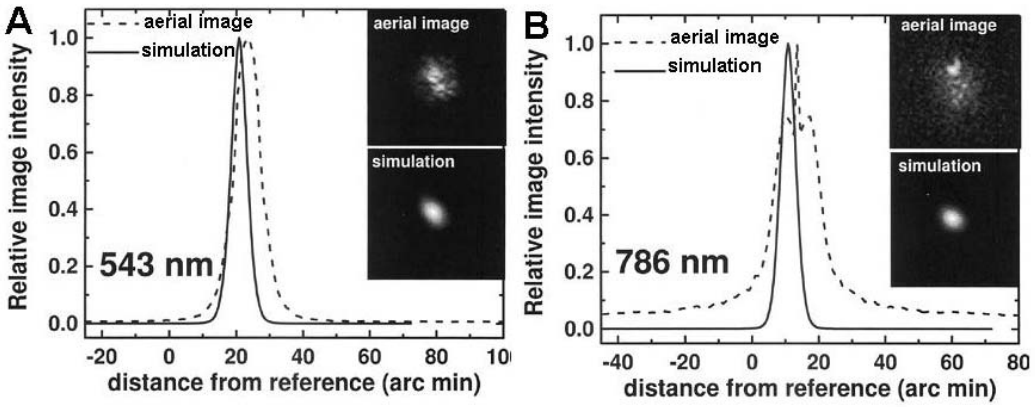

Figure 4.8. Experimental and simulated aerial images for green (A) and infrared (B) light, respectively, for eye #22 and entry pupil at coordinates (+1.5, -2.6 mm). The image on the upper left corner of the plot is the aerial image obtained experimentally, and the image below is the aerial image simulated from measured aberrations as the autocorrelation of first- and second- pass PSFs. The plots represent the normalized radial intensity profile of the corresponding real (dashed) and simulated (solid) aerial images. The distance to zero position represents the centroid deviation from the chief ray. The width of the simulated images accounts for the spread caused exclusively by the measured aberrations, whereas that of the real images also includes other effects, such as scattering and non measured higher-order aberrations, together with the measured aberrations.

The HS images in Figure 4.3 C also suggest a larger contribution of scattered light in IR. A crossed polarization configuration was used, which explains the "polarization cross" pattern observed in green light illumination (see Chapter 3, section 3.4.2) (Marcos et al., 2002b). Green illumination maximizes the light reflected by the photoreceptor outer segments (Elsner et al., 1992) which are thought to partly retain polarization (Gorrand et al., 1984) Light multiply scattered by deeper layers (probably a significant component of the IR images (Elsner et al., 1996)) does not retain polarization, and therefore the HS spots will show

little polarization-related intensity differences across the image (See Chapter 3).

The effects mentioned above affect the shape and intensity distribution of the aerial image and are critical in double-pass measurements of the optical quality of the eye. In this technique, MTF estimates are directly obtained from double-pass aerial images. An appropriate halo subtraction is critical to obtain MTFs in IR consistent to those measured in green light (Lopez-Gil and Artal., 1997). However, reflectometric techniques for wave aberration measurements only rely on centroid deviation computations, which as shown, are not significantly affected by wavelength.

4.5.2.- CHROMATIC DIFFERENCE OF FOCUS

The defocus term was significantly different across wavelengths in all but one subject. The mean focus difference between green and IR across subjects was 0.78±0.29 D, close to the shift estimated by the linear fitting shown in Figure 4.6 (0.72 D). This value agrees well, within the inherent variability, with the chromatic focus shift predicted by the Indiana chromatic reduced eye model (Thibos et al., 1992) (see equation (4.1)).

$$R_E = 633.46 \cdot \left[\frac{1}{(\lambda_G - 214.102)} - \frac{1}{\lambda_{IR} - 214.102} \right] = 0.82\,D \qquad (4.1)$$

where λ_G=543 nm and λ_{IR}=787 nm (mean between IR wavelength used for LRT, 786 nm, and HS, 788 nm).

Thibos et al. (Thibos et al., 1992) obtained the parameters of their eye model by fitting experimental data for a range of wavelengths between 400 nm and 700 nm, and using Cornu's expression for the dependence of the index of refraction with wavelength. Equation (4.1) agrees well with experimental data in the literature for wavelengths up to 760 nm (close to

the wavelength used in this study), with variations close to the intersubject variability in our sample (Thibos et al., 1992). Fernandez et al. (Fernandez et al., 2005) measured the ocular aberrations with wavelengths ranging from 700 to 900 nm for four eyes, and found a good agreement with the values predicted by equation (4.1), even though the wavelength values they used extended even further in the IR. They reported a value for the chromatic difference in defocus between their wavelengths of 0.4 D. A recent study (Fernandez and Artal, 2008) extended the range of wavelengths for measured aberrations even further in the IR (632.8-1070), finding a defocus difference of 1 D. They compared their defocus values for each of the five wavelengths measured with those given by the Cauchy equation, proposed by Atchison and Smith (Atchison and Smith, 2005), for the same wavelengths and found that values corresponding to 1030, 1050 and 1070 nm were located away from the theoretical curve. They thought this difference, supposing that Cauchy equation is still valid in IR, might be due to the deeper penetration and consequent backscattering at this longer wavelengths.

It has been frequently argued that differences in the retinal layer where light is reflected may cause differences between manifest refraction and retinoscopy (Millodot and Sivak, 1979, Millodot, 1980). Charman and Jennings (1976) and Williams et al. (1994) for red light, and later López-Gil and Artal (1997) for near IR light showed that the differences between subjective and reflectometric focus were negligible, and concluded that reflection contributing to the central core of the PSF occurred within the photoreceptor layer. Our results, based on the Zernike defocus term of wave aberration reflectometric estimates, also support this conclusion. The focus shift found is slightly lower than the chromatic shift prediction (by 0.10 D), consistent with a reflection plane behind the photoreceptor layer. However, this shift is of the order of the measurement error (0.12 D for green light and 0.08 D for IR light on average), and lower than the intersubject variability (0.29 D). No particular trend was found for the

focus shift in normal, young subjects as a function of refractive error (coefficient of correlation, r=0.17, p=0.44). In addition, no particular difference was found for the focus shift in eyes with abnormal corneas by LASIK surgery. However, the focus shift found was much higher than the average for the oldest and the aphakic eyes (1.5 D and 1.7 D; eyes #4 and 8, respectively). Although our population did not sample different age groups homogeneously, a slight increase of focus shift with age (r=0.45, p=0.02) was found when including all our subjects. However, the majority of subjects were young or middle-aged (20-43 years old) and no aged-related trend (r=0.26, p=0.20) was found within this age range.

4.5.3.- CONCLUSION

The equivalence of high order aberrations measured in visible or near IR illumination with LRT and HS within the accuracy of the techniques has been shown. The shift found in the defocus term was consistent with the shift predicted by chromatic aberration

These results are relevant because typical commercial wavefront sensing devices and ocular examination devices use IR illumination. It has been shown that despite the longer tails of the aerial images at this wavelength, IR can be successfully used in all the tested conditions, including old and surgical eyes. An experimental value for the focus shift between near IR (786-788 nm) and green (543 nm) illumination in two reflectometric aberrometers (LRT and HS) has also been provided. One of the most promising applications of wavefront sensing devices is their use as sophisticated autorefractometers. They are now being applied for use in refractive surgery to guide ablation with the aim of compensating both low (2^{nd} order aberrations) and HOA aberrations. An accurate transformation of the IR estimates of spherical error into visible wavelengths is crucial to determine the actual correction that should be applied. It has been shown that Thibos's chromatic reduced eye model equation is a valid expression to predict focus shift for our wavelength.

However, for longer wavelengths there is no evidence of the validity of this equation, and new expressions for the refractive index and chromatic difference of refraction may need to be developed. In addition, it has been found that discrepancies can occur in aphakic eyes, and that there might be age-dependent corrections to equation (4.1).

Several reports in the literature found differences in the LCAs of aphakic eyes (Millodot, 1976) and pseudoaphakic eyes (Negishi et al., 2001) with respect to normal eyes. Possible age-related changes of LCA have been a matter of controversy (Howarth et al., 1988, Mordi and Adrian, 1985, Morrell et al., 1991, Calver et al., 1999). Although much of these refractive discrepancies are small, their magnitude can be comparable to that of HOA, and therefore accurate predictions of spherical errors for visible light from IR measurements are important.